Breast tomosynthesis with monochromatic beams: a feasibility study using Monte Carlo simulations

2014 Phys. Med. Biol. 59 4681

(http://iopscience.iop.org/0031-9155/59/16/4681)

IOP Publishing | Institute of Physics and Engineering in Medicine Physics in Medicine & Biology

Phys. Med. Biol. **59** (2014) 4681–4696 doi:10.1088/0031-9155/59/16/4681

Breast tomosynthesis with monochromatic beams: a feasibility study using Monte Carlo simulations

A Malliori[1], K Bliznakova[2], I Sechopoulos[3], Z Kamarianakis[1], B Fei[3] and N Pallikarakis[1]

[1] Department of Medical Physics, Faculty of Medicine, University of Patras, Patras 26500, Greece
[2] Department of Electronics, Technical University of Varna, Varna 9010, Bulgaria
[3] Department of Radiology and Imaging Sciences, Emory University School of Medicine, Atlanta, GA 30322, USA

E-mail: nipa@upatras.gr

Received 25 February 2014, revised 19 May 2014
Accepted for publication 9 June 2014
Published 1 August 2014

Abstract

The aim of this study is to investigate the impact on image quality of using monochromatic beams for lower dose breast tomosynthesis (BT). For this purpose, modeling and simulation of BT and mammography imaging processes have been performed using two x-ray beams: one at 28 kVp and a monochromatic one at 19 keV at different entrance surface air kerma ranging between 0.16 and 5.5 mGy. Two 4 cm thick computational breast models, in a compressed state, were used: one simple homogeneous and one heterogeneous based on CT breast images, with compositions of 50% glandular–50% adipose and 40% glandular–60% adipose tissues by weight, respectively. Modeled lesions, representing masses and calcifications, were inserted within these breast phantoms. X-ray transport in the breast models was simulated with previously developed and validated Monte Carlo application. Results showed that, for the same incident photon fluence, the use of the monochromatic beam in BT resulted in higher image quality compared to the one using polychromatic acquisition, especially in terms of contrast. For the homogenous phantom, the improvement ranged between 15% and 22% for calcifications and masses, respectively, while for the heterogeneous one this improvement was in the order of 33% for the masses and 17% for the calcifications. For different exposures, comparable image quality in terms of signal-difference-to-noise ratio and higher contrast for all features was obtained when using a monochromatic 19 keV beam at a lower mean glandular dose, compared to the polychromatic one. Monochromatic images also provide better detail and, in

combination with BT, can lead to substantial improvement in visualization of features, and particularly better edge detection of low-contrast masses.

Keywords: breast tomosynthesis, monochromatic beams, monte carlo, modeling, simulation

(Some figures may appear in colour only in the online journal)

1. Introduction

Breast Tomosynthesis (BT) is a pseudo-three-dimensional (3D) x-ray imaging technique of the breast that reconstructs tomographic images from a set of angular projections taken in an arc around the breast (Niklason *et al* 1997). The advantage of BT imaging over conventional mammography is the depiction of breast structures with a substantial reduction in tissue superposition. This technique is especially valuable for patients with breasts characterized as heterogeneously dense or extremely dense (Baker and Lo 2011). Large-scale clinical studies showed BT being valuable in evaluation of benign (cysts, fibroadenomas) and malignant masses, architectural distortions and asymmetries. Clinical studies with BT have shown the ability of this technique to improve the detection and characterization of suspicious lesions, especially low-contrast masses, at doses similar to the ones used in conventional x-ray two-dimensional (2D) mammography (Dobbins 2009, Poplack *et al* 2007). At the same time, some tomosynthesis clinical studies have shown some problems when detecting small calcifications (Cs) while others have shown equivalent performance compared to mammography. Due to the limited number of projection images, the high-contrast Cs can cause artifacts that appear on other slices as multiple repeating out-of-plane ghost images.

In general, average glandular doses for a single BT acquisition are reported to vary between 0.6 and 4.0 mGy (Dobbins 2009, Feng and Sechopoulos 2012, Poplack *et al* 2007). However, the radiation dose depends not only on the exam itself, but also on whether the tomosynthesis exam will be combined with mammography. As a screening technology, reducing the radiation dose required for BT acquisition with no loss or even improvement of image quality is always desirable. One way to obtain this is through the use of monochromatic beams with BT. In conventional mammography, the produced x-ray energies are in the interval 10–32 keV. Typically, molybdenum (Mo), rhodium (Rh) or tungsten (W) anodes are used in combination with Mo, Rh, aluminium or silver filters (Dance *et al* 2000a). Although K-edge filtration and optimization of the x-ray tube parameters and spectrum are known to significantly reduce the dose (Bernhardt, Mertelmeier and Hoheisel 2006, Dance *et al* 2000b, Thilander-Klang *et al* 1997), a considerable number of low energy photons remain, and filtration is limited by the resulting low fluence rate. Previous investigations, in the field of 2D mammography, have demonstrated that the contrast of objects such as lesions or contrast media can be enhanced considerably by using monochromatic x-rays in the range of 17–24 keV, instead of polychromatic beams (Diekmann *et al* 2004, Hoheisel *et al* 2005) at much lower doses (Baldelli *et al* 2003, 2004, 2005, Yoon *et al* 2012). Photons with energies higher than 24–25 keV penetrate the soft tissue deeper and are more likely to undergo Compton scatter, while the probability of undergoing photoelectric effect decreases, resulting in mammograms with reduced contrast. On the other hand, photons with energies below 17 keV are more readily absorbed by the soft tissues. Therefore, at lower energies, in order to obtain adequate transmission through the breast and produce an image with an acceptable signal to noise ratio, more incident radiation must be used, resulting in a higher mean glandular dose.

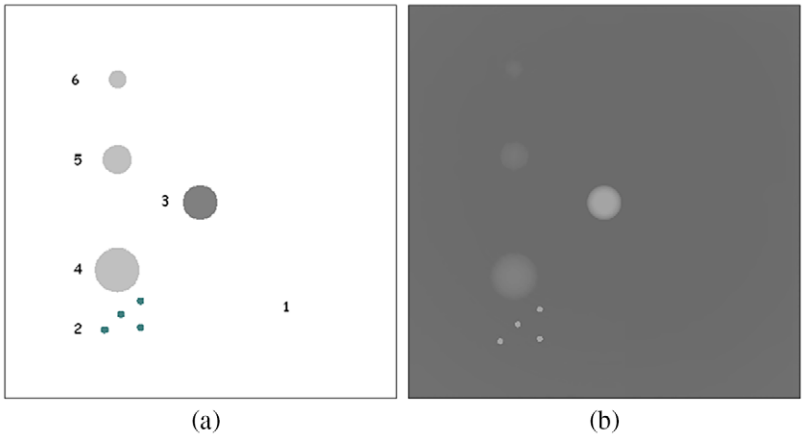

Figure 1. Simple phantom: (*a*) schematic representation of the arrangement of features in the phantom. Features 3–6 are low-contrast objects that approximate breast masses, 2 is a group of high-contrast objects that represent Cs, 1 is the breast tissue of the homogeneous phantom of 50% glandularity (dimensions are specified in detail in table 1); (*b*) noise-free projection image of the phantom.

At the same time, the use of monochromatic beams may improve the appearance of small Cs and mass characterization due to better edge depiction. However, the studies reported up to now are limited by the use of homogeneous mammographic phantoms. Another study that compared monochromatic and polychromatic beams included the use of Monte Carlo techniques and a software anthropomorphic phantom (Muller *et al* 2011). This study demonstrated improved contrast and noise characteristics of images acquired with a monochromatic beam compared to those using a polychromatic beam. This is actually the only reported qualitative comparison up to date.

These few studies point to the potential of using monochromatic beams with BT. Simulation and experimental studies that evaluate directly the feasibility of BT with monochromatic beams, have not been reported up to date. In particular, critical in this assessment, is the inclusion of noise from both anatomical and quantum noise sources, as both limit mass conspicuity in clinical images.

Therefore, the aim of this study is to investigate the impact of using monochromatic beams on image quality for lower dose BT. For this purpose, we performed modeling and simulation of BT and mammography imaging processes and evaluated the results in terms of signal-difference-to-noise ratio, contrast and a figure of merit equal to the signal-difference-to-noise-ratio normalized by the square root of the mean glandular dose.

2. Materials and methods

2.1. Software phantoms

2.1.1. Simple phantom. A 4 cm-thick software phantom, with a homogenous background of 50% glandular and 50% adipose tissue, was designed (figure 1(*a*)) with the in-house developed software XRayImagingSimulator (Bliznakova *et al* 2010). The value corresponding to each voxel is determined by the tissue dominant in that voxel. The voxel size is 0.1 mm in each direction. Figure 1(*b*) shows an ideal projection image of the square phantom, obtained with a 19 keV monochromatic beam and showing the features of interest that are placed in the middle

Table 1. Simple homogenous and complex heterogeneous breast phantom characteristics.

	Object	Type	Dimensions
Simple phantom	1	Breast tissue (50% gland/50% adipose)	[*x*,*y*,*z*] $70 \times 70 \times 40\,\text{mm}^3$
	2	Group of 4 Cs ($CaCO_3$)	diameter 1.0 mm
	3	Spherical water insert	diameter 6.0 mm
	4	Glandular mass (75% gland/25% adipose)	diameter 8.0 mm
	5	Glandular mass (75% gland/25% adipose)	diameter 5.0 mm
	6	Glandular mass (75% gland/25% adipose)	diameter 3.0 mm
CT based breast phantom	1	Breast tissue (40% gland/60% adipose)	$175 \times 48 \times 134\,\text{mm}^3$
	2	Water insert with irregular margins	diameter 8.5 mm
	3	Group of 6 Cs ($CaCO_3$)	diameter 1.3 mm
	4	Group of 6 Cs ($CaCO_3$)	diameter 1.0 mm
	5	Group of 6 Cs ($CaCO_3$)	diameter 0.4 mm
	6	Group of 5Cs ($CaCO_3$)	diameter 0.2 mm

plane of the phantom (at 20 mm above the phantom base). These features are Cs and breast masses of various sizes and densities. Their characteristics are described in detail in table 1.

2.1.2. CT breast phantom. A 3D software breast model with realistic breast tissue distribution was created from slices, obtained from a dedicated breast CT scanner at the Department of Radiology and Imaging Sciences at Emory University (Atlanta, Georgia, USA). Initially, the data were de-noised and segmented in order to obtain a compositional breast model composed of skin, glandular, and adipose tissues (Yang *et al* 2012, Yang, Sechopoulos and Fei 2011). The voxel size of the 3D breast model was 0.28 mm in each direction; the whole breast volume was calculated to be 380 ml, placed in a 3D matrix with size of $175 \times 48 \times 134\,\text{mm}^3$. The glandular portion occupied 37% of the breast volume. A compressed version was created from this volume using the compression algorithm (Zyganitidis, Bliznakova and Pallikarakis 2007). The compression plates were placed at a position to generate a breast with 4 cm compressed thickness. For densities $\rho_{\text{gland}} = 1.04\,\text{g cm}^{-3}$ and $\rho_{\text{adipose}} = 0.93\,\text{g cm}^{-3}$, (Hammerstein *et al* 1979) the mixture by weight of glandular and adipose tissue for this phantom was found to be 40% and 60%, respectively. Further, four clusters of Cs and a water insert, simulating a breast mass with irregular margins (generated using the methodology presented in Hintsala *et al* 2010) were inserted within the 3D computational breast model, all placed in the middle of the phantom (at 20 mm above the phantom base). Figure 2(*a*) presents schematically the arrangement of the breast abnormalities inserted in the volume, while figure 2(*b*) shows a noise-free projection image of the breast phantom obtained with a monochromatic beam of 19 keV, using the analytical module of the XRayImagingSimulator (Bliznakova *et al* 2010). This projection image depicts the breast tissue, the breast lesion and four groups of Cs with gradually decreasing diameters of 1.3, 1, 0.4, and 0.2 mm. The characteristics of the phantom are summarized in table 1.

2.2. Acquisition simulation

The acquisition geometry for the simulation of BT, shown in figure 3(*a*), was equivalent to that of the Siemens Mammomat Inspiration System. The acquisition scan included 25 equally

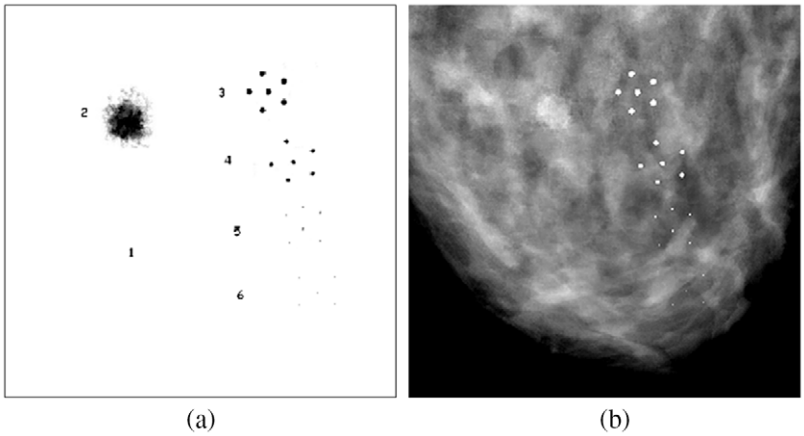

Figure 2. Software breast model from patient breast CT slices: (*a*) schematic representation of abnormalities included in the phantom: 2 is a water insert representing an irregular breast mass, 3–6 are groups of Cs and 1 is the breast tissue of the heterogeneous phantom of 40% glandularity; (*b*) noise-free 2D mammographic image simulated at craniocaudal view, showing the breast tissue composition, the irregular lesion and the four groups of Cs.

spaced x-ray projection images simulated within a limited arc of 50°. Source-to-isocenter distance (SID) was 600 mm, while source to detector distance (SDD) was 665 mm. Images with a size of 480 × 480 square pixels with a pitch of 170 μm were simulated for the simple phantom and images of 800 × 800 square pixels with a pitch of 200 μm were simulated for the complex heterogeneous phantom, respectively (table 2). The pixel dimensions were chosen as a trade-off between computational time and resolution of objects on images that should be enough for performing image quality evaluation. In addition, images of selected regions of interest (ROIs) from the simple homogeneous phantom were simulated with higher resolution i.e. 50 μm. This pixel resolution was chosen as a realistic resolution that may be obtained at a synchrotron facility.

X-ray interactions in both breast models were simulated using an in-house developed Monte Carlo x-ray simulation software package (Lazos *et al* 2003). This program has been reworked for voxel-based phantoms and adjusted for mammography simulations (Bliznakova *et al* 2012). The program followed the histories of single photons, emitted from the x-ray source as they pass through the breast phantom and then reach the detector. Photon transport is modeled on the Monte Carlo methods. The distance between two successive interactions is sampled, based on the relevant attenuation cross-sections, accounting for the different media along the photon path. For the used mammographic x-ray energy range, three interaction processes are considered—the photoelectric effect, the coherent and the incoherent scattering. Any time an interaction occurs inside the phantom, one of the three interaction processes is selected by random sampling, according to the relative cross-sections of the processes at the specific photon energy and medium (Lazos *et al* 2003). The dose is calculated in Cartesian voxels as described previously. The energy deposited by photons and electrons in each voxel that contained gland tissue is accumulated and consequently is divided by the mass of this voxel. This results in a total glandular dose per voxel. The total mean glandular dose (MGD) was computed by averaging all dose per voxel values over the entire glandular volume, as described in Yi *et al* (2011). For the homogeneous case, each voxel of the breast volume that does not contain simulated abnormality, comprised a mixture of 50% adipose and 50%

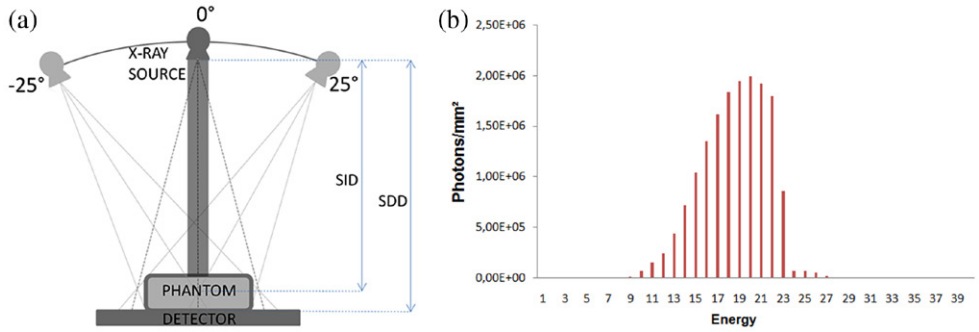

Figure 3. Simulated BT and 2D mammography acquisition geometry: (*a*) schematic representation of the acquisition system (*b*) simulated 28 kVp W/Rh mammographic spectrum.

Table 2. Acquisition scenarios for both 2D mammography and BT. In case of BT, 25 projection images are acquired in the range (−25° to 25°).

Phantom	Beam Type	Photons per mm^2	Image size (pixels), pixel size
Simple phantom	28 kVp W/Rh	8.10×10^5	
		8.10×10^6	480×480, 170 μm
		1.62×10^7	480×480, 50 μm
		2.43×10^7	
	19 keV	8.10×10^5	
		8.10×10^6	480×480, 170 μm
		1.62×10^7	480×480, 50 μm
		2.43×10^7	
CT based breast phantom	28 kVp W/Rh	1.62×10^7	800×800, 200 μm
		2.43×10^7	
	19 keV	1.62×10^7	800×800, 200 μm
		2.43×10^7	

glandular weighted by mass. Based on that, the MGD was scored. To speed up the simulations, parallel execution on GPU was adapted. With this configuration, the time needed to produce a synthetic mammogram of the simple and complex phantoms for the highest photon fluence was 10 and 30 h, respectively.

The synthetic mammograms simulated with this acquisition geometry, represent 2D spatial distribution of the energy of the x-rays that pass the breast model and reach the front part of the detector. The images are synthesized for a monochromatic beam of 19 keV and for a common 28 kVp tungsten (W) target and 50 μm rhodium (Rh) filter mammographic spectrum (Boone 1998, Boone, Fewell and Jennings 1997) with a mean energy of 18.8 keV and a first HVL = 0.454 mm Al. In both monochromatic and polychromatic cases, the total number of photons was kept the same and equal to 1.62×10^7 photons mm^{-2}. The spectrum representing the distribution of the number of photons per energy level is shown in figure 3(*b*). In the case of BT, the total number of photons used for the 2D mammogram was equally distributed in the 25 projection images. Additional levels of incident photon fluence were simulated as listed in table 2. In the present x-ray simulations, an ideal detector was assumed, while an anti-scatter grid and compression plates were not considered.

Entrance surface air kerma (ESAK) is calculated as the photon fluence after the filter (photons mm^{-2}) over the photon fluence per mR in air and then converted to mGy.

In addition to estimating the MGD from our Monte Carlo simulations, we also estimated MGD for all simulated image acquisitions using previously published models. For monochromatic beams, the MGD was calculated as MGD = ESAK × g, where g is the incident air kerma to MGD conversion factor from Boone (2002). For a polychromatic beam, the MGD was calculated as MGD = ESAK × g × c × s from Dance *et al* (2000a). In this model, the factor c corrects for any difference from 50% glandularity in breast composition, and s corrects for any difference from the original tabulation by Dance (1990) due to the use of a different x-ray spectrum factor. Specifically, the c value for 40% glandular tissue was estimated by linear interpolation between the g values provided for 25% gland and 50% gland and the s factor was set to 1.042 for the W/Rh spectrum.

A simple backprojection method was used as a tomosynthesis reconstruction algorithm. The method has been realized in an in-house developed software platform, dedicated for x-ray imaging reconstructions. Projection filtering prior to the reconstruction was not applied. Tomosynthesis slices were separated by 1 mm.

2.3. Image quality evaluation metrics

The variation of several image characteristics: signal difference to noise ratio, contrast and figure of merit is investigated for all images.

The signal difference to noise ratio (SDNR) is defined as:

$$SDNR = \frac{\left|\bar{\mu}_f - \bar{\mu}_{bk}\right|}{\sigma_{bk}} \tag{1}$$

where $\bar{\mu}_f$ is the average value of the feature, while $\bar{\mu}_{bk}$ and σ_{bk} are the average and standard deviation values of the background, respectively.

The contrast (C) is calculated as:

$$C = \frac{\left|\bar{\mu}_f - \bar{\mu}_{bk}\right|}{\bar{\mu}_{bk}} \times 100\% \tag{2}$$

for a given beam quality. If the system is quantum limited, SDNR is proportional to the square root of the incident exposure to the breast or to the MGD. Therefore, in this study we used the following figure of merit (FOM) to normalize the SDNR by the MGD in order to allow the comparison of results derived from different dose measurements:

$$FOM = \frac{SDNR}{\sqrt{MGD}} \tag{3}$$

For the homogeneous phantom, the average value was calculated over a circular ROI inside each feature with a diameter of 35 pixels (5.8 mm), 25 pixels (4.2 mm) and 4 pixels (0.7 mm) for the water insert (6 mm diameter), the glandular mass (5 mm) and the Cs (1 mm), respectively. The properties of the background ($\bar{\mu}_{bk}$ and σ_{bk}) were evaluated for asquare area of 60 × 60 pixels (10 × 10 mm^2) located between the water insert and the two bigger glandular masses. In the case of the heterogeneous phantom, the background ROI analyzed was a rectangular 30 × 40 mm^2 area of breast tissue located in the space between the chest wall and the groups of Cs. For the water insert simulating an irregular mass (8.5 mm), a circular ROI of 5.5 mm diameter inside the feature was analyzed and the mean value of the pixels was calculated as $\bar{\mu}_f$. Similarly, for the Cs, circular ROIs inside each feature were defined. For Cs belonging to the two bigger groups (1.3 and 1 mm), for each feature was calculated from the mean value of the pixels inside ROIs of diameters 0.8 and 0.6 mm respectively. For Cs belonging to the two

Table 3. ESAK and MGD dose calculations.

Phantom	Beam Type	Incident photon fluence (Photons mm $^{-2}$)	ESAK (mGy)	MGD (mGy) comparison estimations[a]	MGD_{MC} (mGy) Monte Carlo 2D[b]	MGD_{MC} (mGy) Monte Carlo BT[b]
Simple phantom	28 kVp W/Rh	8.10×10^5	0.18	0.06	0.05	0.05
		8.10×10^6	1.83	0.56	0.53	0.52
		1.62×10^7	3.66	1.11	1.05	1.04
		2.43×10^7	5.49	1.67	1.58	1.57
	19 keV	8.10×10^5	0.16	0.06	0.05	0.05
		8.10×10^6	1.56	0.57	0.55	0.54
		1.62×10^7	3.13	1.13	1.10	1.09
		2.43×10^7	4.69	1.70	1.65	1.64
CT breast phantom	28 kVp W/Rh	1.62×10^7	3.66	1.16	1.29	1.27
		2.43×10^7	5.49	1.73	1.93	1.91
	19 keV	1.62×10^7	3.13	1.17	1.35	1.34
		2.43×10^7	4.69	1.76	2.03	2.00

[a] (Boone 2002, Dance 1990, Dance *et al* 2000).
[b] Current study.

smaller groups, areas that contained each feature were defined and the maximum value was extracted and used asin each case.

3. Results and discussion

3.1. Dose evaluation

Table 3 summarizes the ESAK values and the mean glandular dose estimations using the previously published models and our own Monte Carlo simulations.

Our Monte Carlo estimates were close to the estimations using the Dance and Boone models (table 3). Dose calculations revealed that, for equal exposure, ESAK was higher in the polychromatic case by 17% compared to monochromatic, while the MGD values were very similar.

3.2. Polychromatic versus monochromatic beams for equal incident photon fluence

3.2.1. Simple phantom. A comparison of 2D mammographic images and BT slices, obtained with monochromatic 19 keV and polychromatic 28 kVp x-ray beams, is shown in figure 4. These images have been acquired using the simple phantom with photon fluence of 1.62×10^7 photons mm $^{-2}$ and detector pixel size equal to $170 \times 170\,\mu m^2$. Regions of interest from 2D projection images with monochromatic 19 keV and polychromatic 28 kVp obtained for a detector pixel size of 50 μm and the same photon fluence of 1.62×10^7 photons mm $^{-2}$ are shown in figure 5.

It can be observed from figures 4 and 5 that images obtained with monochromatic and polychromatic beams are similar in their visual appearance. However, in the case of a monochromatic beam, the breast masses are characterized by improved detection and visualization for both mammography and BT. These large low-contrast features have attenuation coefficients close to that of the breast tissue, which makes it harder to distinguish them from the background compared to the group of Cs. The in-plane resolution of the system, measured using the Cs in the phantom, was similar when using monochromatic and polychromatic beams (slightly

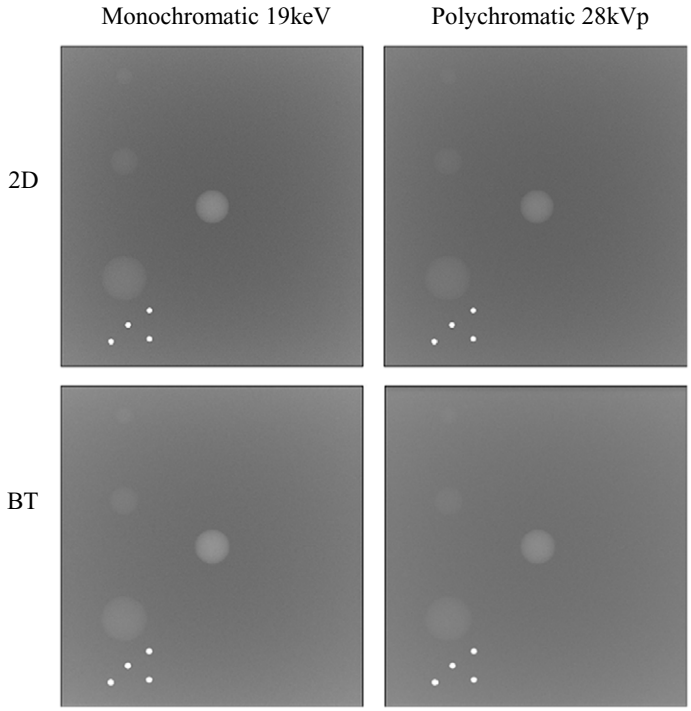

Figure 4. Simulated monochromatic 19 keV (left) and polychromatic 28 kVp (right) images of the simple phantom: 2D mammography images (upper row) and BT slices (lower row) for photon fluence of 1.62×10^7 photons mm^{-2}. Detector pixel size was 170 μm.

better for monochromatic with 5% smaller FWHM). Additionally, an 11% improvement in depth resolution was found for the monochromatic beam. Further, features in 2D images and tomosynthesis slices were evaluated quantitatively by calculating SDNR, C and FOM for both monochromatic and polychromatic x-ray beams. Figures 6(*a*)–(*c*) shows the corresponding SDNR, C and FOM graphs of the spherical water insert (6 mm), glandular mass (5 mm) and group of Cs (1 mm) visible on the 2D images and BT slices. For the case of Cs, the values that are presented correspond to the average values of the four Cs. The quantitative results presented are for images acquired with 1.62×10^7 photons mm^{-2} and pixel size of 170 μm.

The quantitative analysis shows that monochromatic beam results in higher image quality compared to polychromatic for all figures of merit (SDNR, C and FOM), confirming the visual observations. The percentage of the SDNR improvement of monochromatic over polychromatic is similar for both 2D and BT sets (slightly higher in case of BT) and varied between 14% and 23% with the highest benefit observed for the water mass and less improvement for the Cs group. The corresponding FOM values were increased by 12% for the group of Cs, 13% for the glandular mass and 20% for the water insert, while the improvement in C values was higher and ranged between 15% and 22%.

The comparison between BT and 2D imaging showed lower C values for BT compared to 2D case. However, BT performed with monochromatic beam, has comparable or higher (in case of the masses) C values than polychromatic 2D conventional mammography.

3.2.2. CT breast phantom. Similarly to the simple breast phantom case, figure 7 shows the 2D and the tomosynthesis slices for the heterogeneous CT-based breast phantom obtained with

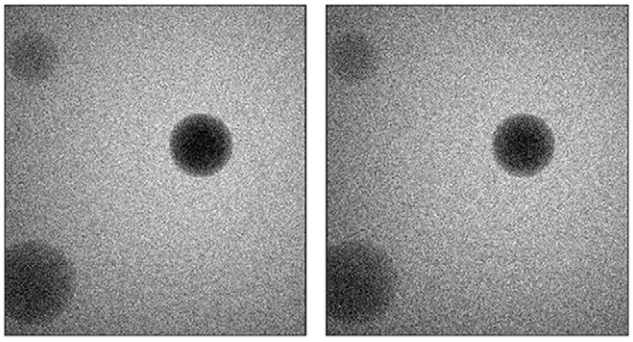

Figure 5. ROIs from simulated 2D projection images of the simple phantom obtained with monochromatic 19 keV (left) and polychromatic 28 kVp (right) beams, for photon fluence of 1.62×10^7 photons mm^{-2}. Detector pixel size was 50 μm.

simulation of monochromatic and polychromatic beams with a photon fluence of 1.62×10^7 photons mm^{-2} and detector pixel size equal to 200 μm.

It can be observed that the visibility of the features of interest, and especially of the low-contrast mass, is much improved in the BT images compared to the 2D in the case of the heterogeneous breast phantom. Overlying breast anatomy in 2D images hides the borders and shape of the mass and makes it difficult to detect its irregular shape, which is very important for the characterization of lesions. Moreover, acquisition with the monochromatic beam resulted in increased contrast and thus better detection and visualization of all features.

Figures 8(*a*), (*b*) depicts the quantitative evaluation for 2D and BT images with monochromatic and polychromatic x-ray beams. The features that were evaluated are the irregular mass with size of 8.5 mm and the four groups of Cs. For the case of Cs, the values presented correspond to the average values of the four groups Cs (1.3, 1, 0.4 and 0.2 mm). The results are from images acquired with 1.62×10^7 photons mm^{-2} and 200 μm resolution.

The benefit of BT in case of breasts with heterogeneous background can be seen in the results shown in figure 8. Apart from the visual improvement that was observed in the images, quantitative analysis confirms the improvement with an increase in SDNR values for the case of water insert and groups of Cs. Unlike SDNR, the C values are reduced in BT compared to 2D, but still monochromatic BT is better than polychromatic 2D, similarly to the case of simple homogeneous breast phantom.

Although the use of a monochromatic beam improves image quality, in the case of heterogeneous phantoms, both the lesions and the anatomical structure of the background are enhanced, the latter increasing the standard deviation of the background. This can explain the lower SDNR and FOM improvement of monochromatic images compared to the case of simple phantom (homogeneous background), despite the improved visibility of the features of interest in both cases. Thus, for the case of the breast phantom with realistic tissue distribution, the use of a monochromatic beam yields benefits, mainly in C. An increase of 33.4% and 17% is achieved from the monochromatic BT compared to the polychromatic BT for the low and high-contrast features, respectively. The corresponding contrast improvement between monochromatic and polychromatic acquisitions in the 2D case is similar i.e. 30.7% and 15%.

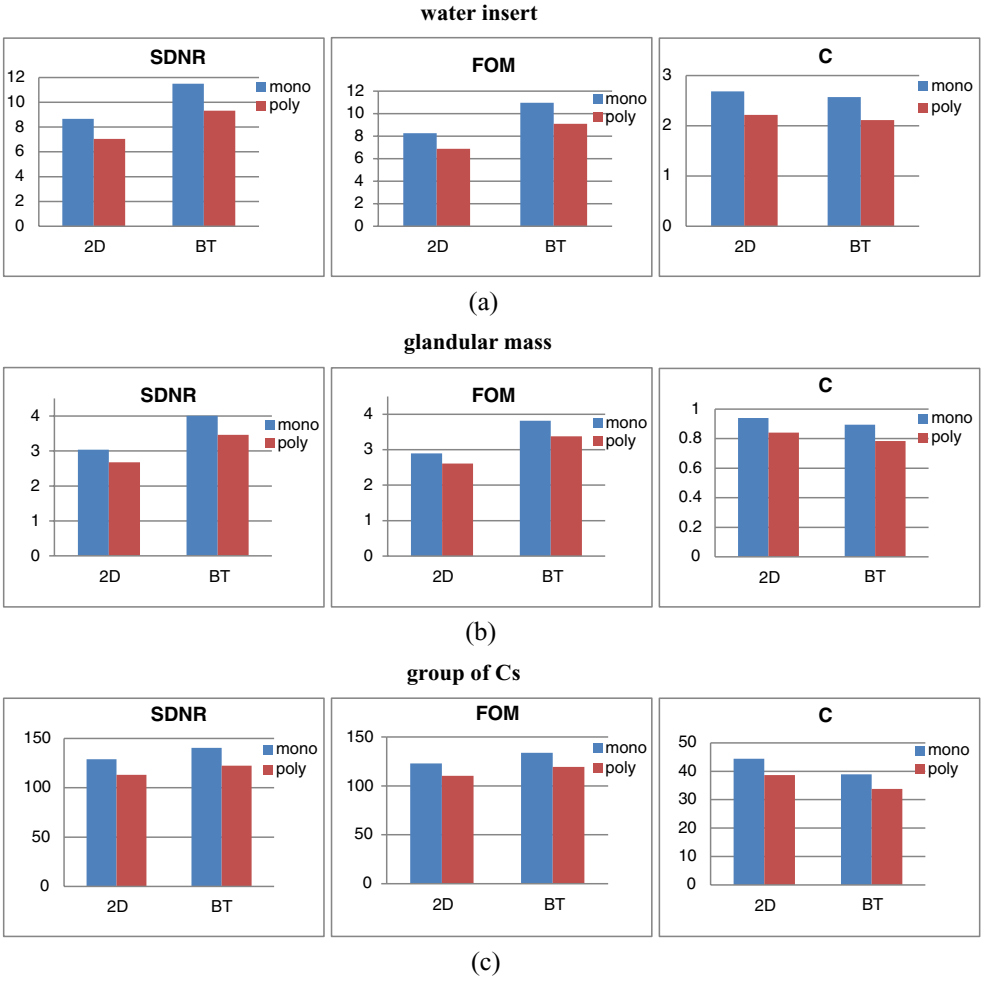

Figure 6. Evaluation performed on 2D and BT images of the simple phantom acquired with monochromatic and polychromatic beam (photon fluence of 1.62×10^7 photons mm $^{-2}$ and pixel size of 170 μm). SDNR, FOM and C graphs for (*a*) water insert with size of 6 mm, (*b*) glandular mass with size of 5 mm and (*c*) Cs with size of 1 mm.

3.3. Low dose tomosynthesis: simulation studies with different ESAK

Initial results suggest that the improved image quality of using a monochromatic beam could allow for acquisitions with lower doses. Visual comparison showed that in all cases, features were better visualized in monochromatic images compared to the polychromatic ones of the same photon fluence, as in the case demonstrated in figure 4 for 1.62×10^7 photons mm $^{-2}$.

As can be seen in figure 9, SDNR improves with the increase in the MGD as expected, while the C was found to be almost constant (data not shown due to the very close values for the five doses evaluated and not affected with the dose increase). The SDNR-dose graphs show that by using monochromatic beam, we can achieve SDNR values comparable to polychromatic acquisition but with lower MGD (and ESAK). Specifically, comparable SDNR values for the case of breast masses and Cs can be obtained when using monochromatic beam with an incident exposure that results in a MGD that is 1.5 times lower than when using a polychromatic beam.

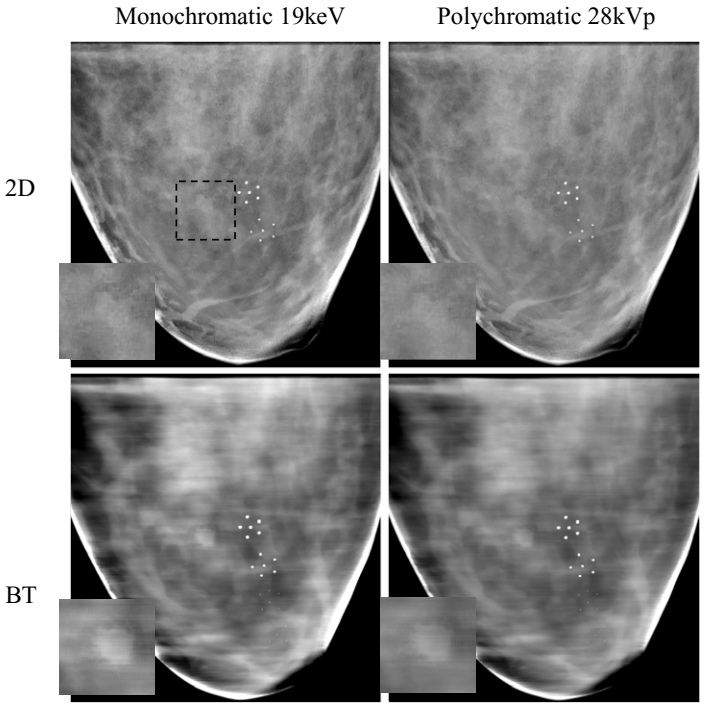

Figure 7. Monochromatic 19 keV (left) and polychromatic 28 kVp (right) images: 2D (upper row), BT (lower row) of the complex breast phantom for photon fluence of 1.62×10^7 photons mm $^{-2}$ and detector pixel size of 200 μm. In the inserts of the 2D and BT images, ROIs that contain the irregular mass are presented.

The above quantitative results are well demonstrated in figure 10. Specifically, figures 10(*a*), (*b*) shows the monochromatic and polychromatic BT slices corresponding to equal incident photon fluence of 2.43×10^7 photons mm $^{-2}$ with the former showing advantage in feature visualization and image quality, as discussed in section *3.2.1* (for equal photon fluence of 1.62×10^7 photons mm $^{-2}$), while figure 10(*c*) is the monochromatic BT slice acquired with the lower incident photon fluence of 1.62×10^7 photons mm $^{-2}$. This image has comparable noise characteristics to the polychromatic one and also an increase of 15–22% in C for the different features evaluated, achieved with MGD that is 1.5 times lower than the MGD obtained with the polychromatic beam.

Similarly, images acquired using these two different exposures for the complex phantom, are presented. Figures 11(*a*), (*b*) shows the polychromatic 2D and BT images corresponding to 2.43×10^7 photons mm $^{-2}$, while figure 11(*c*) is the monochromatic BT image simulated with lower incident photon fluence (1.62×10^7 photons mm $^{-2}$) that resulted in lower (1.5 times) MGD.

The comparison between the polychromatic BT and the monochromatic BT (figures 11(*b*), (*c*)) shows comparable noise characteristics and a C improvement of 33% and 17% for the mass and the Cs, respectively for the case of monochromatic BT with an incident exposure that results in a lower (1.5 times) MGD compared to the polychromatic BT.

The results obtained in these simulations are encouraging for the development of a tomosynthesis system based on monochromatic beams. Such a preclinical setup has been already accomplished at Elettra and was used in our previously reported study (Malliori *et al* 2012). In that case, the phantom was placed on a stage that moved vertically during each image

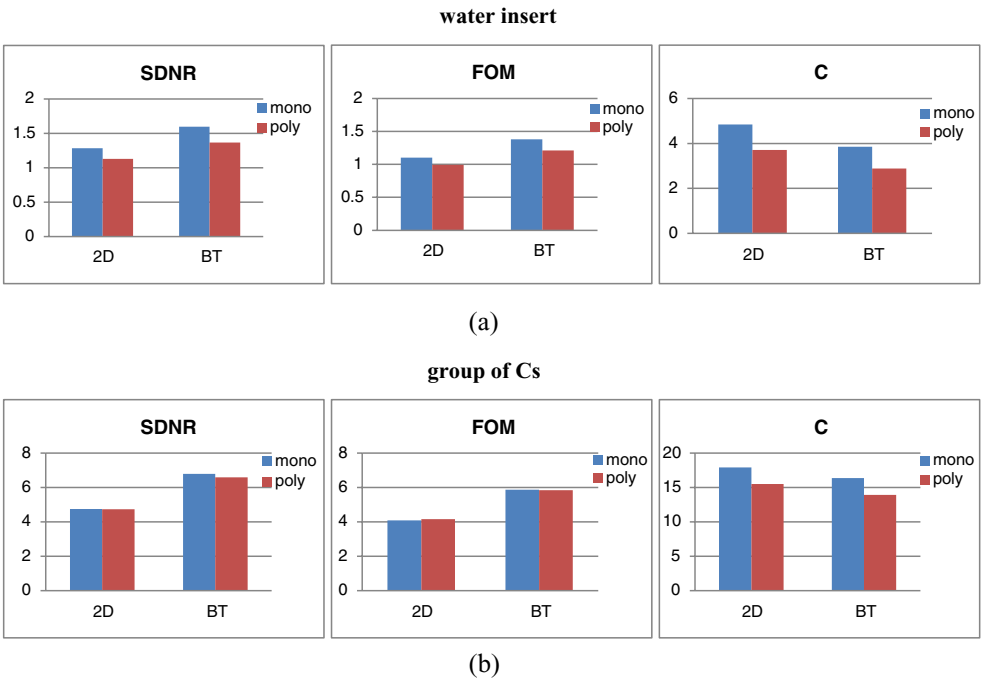

Figure 8. Evaluation performed on 2D and BT images of the heterogeneous CT-based breast phantom simulated with monochromatic and polychromatic beam (photon fluence of 1.62×10^7 photons mm $^{-2}$ and pixel size of 200 μm). SDNR, FOM and C graphs for (*a*) irregular mass with size of 8.5 mm and (*b*) 4 groups of Cs.

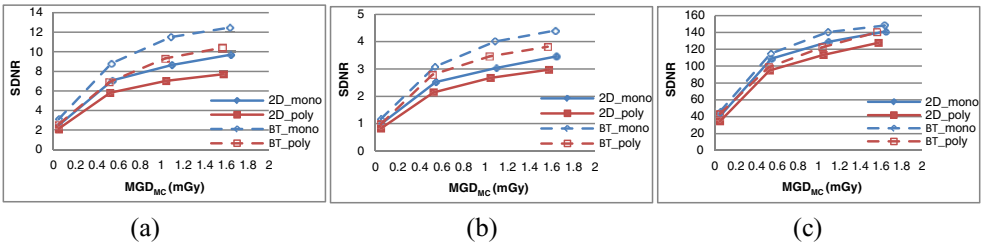

Figure 9. Evaluation of SDNR for different MGD_{MC} levels for 2D and BT images with monochromatic and polychromatic x-ray beams for the simple phantom (*a*) water insert, (*b*) glandular mass and (*c*) group of Cs.

acquisition and rotated in order to obtain images at each specified angle. Presently, at the SYRMEP beamline at Elettra, a synchrotron radiation clinical program in mammography is running. For the purposes of the program, in the patient room, the patient lays prone on a high precision movement support, which includes a special opening for the breast with the size and shape of the aperture consistent with the chest anatomy. The movement system is equipped with three motion stages: horizontal for positioning, vertical for scanning and rotational along an axis perpendicular to the beam for oblique breast projection (Abrami *et al* 2005). This setup may be applicable for breast tomosynthesis. An important limitation factor could be resolution loss and possibly motion artifacts due to breast movement during table rotation. Usually acquisition of one projection image takes a few seconds; thus a set of 11 or 15 images may

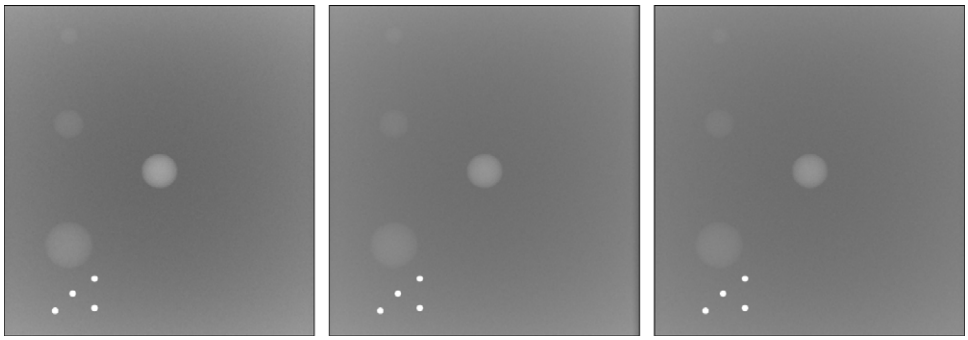

(a) (b) (c)

Figure 10. BT images showing the simple homogeneous breast phantom: (*a*) monochromatic image, photon fluence = 2.43 × 10^7 photons mm $^{-2}$, MGD_{MC} = 1.64 mGy, (*b*) polychromatic image, photon fluence = 2.43 × 10^7 photons mm $^{-2}$, MGD_{MC} = 1.57 mGy and (*c*) monochromatic image, photon fluence = 1.62 × 10^7 photons mm $^{-2}$, MGD_{MC} = 1.09 mGy. Detector pixel size was 170 μm.

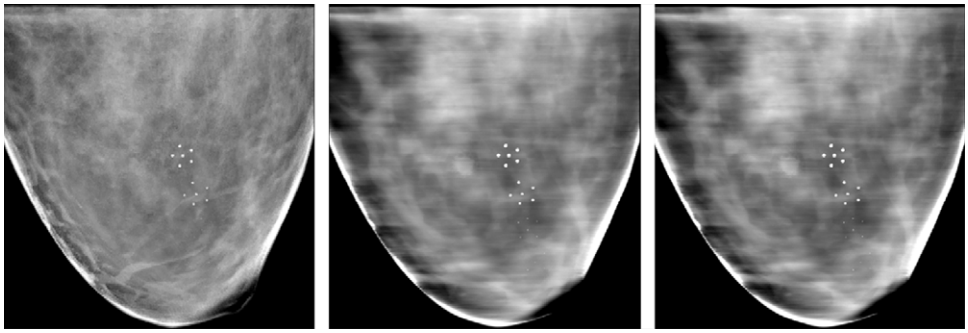

(a) (b) (c)

Figure 11. Simulated images showing the heterogeneous CT-based breast phantom: (*a*) polychromatic 2D image, photon fluence = 2.43 × 10^7 photons mm $^{-2}$, MGD_{MC} = 1.93 mGy, (*b*) polychromatic BT image, photon fluence = 2.43 × 10^7 photons mm $^{-2}$, MGD_{MC} = 1.91 mGy and (*c*) monochromatic BT image, photon fluence = 1.62 × 10^7 photons mm $^{-2}$, MGD_{MC} = 1.34 mGy. Pixel size was 200 μm.

take up to 3–4 min. For such a relatively long image acquisition time, avoiding or correcting for motion could be challenging. Although such challenges currently exist, future technological advances could lead to the realization of monochromatic breast tomosynthesis imaging systems at synchrotron facilities.

4. Conclusions

In this study the impact on image quality of using monochromatic beams for BT imaging was investigated. Results indicate that monochromatic beams could enable a reduction of dose in tomosynthesis without compromising image quality in terms of SDNR or could even result in an increase in C. Monochromatic images can provide better detail and tissue differentiation and in combination with BT can lead to improvement in mass detection and visibility

of borders, which is important for the characterization of the masses, especially when they are spiculated. Overall, monochromatic BT results in improved image quality compared to conventional mammography (polychromatic 2D) in most features evaluated, in addition to providing useful depth information.

Acknowledgements

This research has been co-financed by the European Union (European Social Fund—ESF) and Greek national funds through the Operational Program 'Education and Lifelong Learning' of the National Strategic Reference Framework (NSRF)—Research Funding Program: Heracleitus II. Investing in knowledge society through the European Social Fund. K Bliznakova was partially supported by Marie Curie Career Integration Grant within the 7th European Community Framework Programme, PHASETOMO (PCIG09-GA-2011–293846). I Sechopoulos and B Fei were supported in part by NIH grant R01CA163746 and Susan G Komen Foundation Grant IIR13262248. B Fei was partially supported by NIH grants (R01CA156775 and R21CA176684) and Georgia Cancer Coalition Distinguished Clinicians and Scientists Award.

References

Abrami A *et al* 2005 Medical applications of synchrotron radiation at the SYRMEP beamline of ELETTRA *Nucl. Instrum. Meth.* A **548** 221–7

Baker J A and Lo J Y 2011 Breast tomosynthesis: state-of-the-art and review of the literature *Acad. Radiol.* **18** 1298–310

Baldelli P, Taibi A, Tuffanelli A and Gambaccini M 2003 Quasi-monochromatic x-rays for diagnostic radiology *Phys. Med. Biol.* **48** 3653–65

Baldelli P, Taibi A, Tuffanelli A and Gambaccini M 2004 Dose comparison between conventional and quasi-monochromatic systems for diagnostic radiology *Phys. Med. Biol.* **49** 4135–46

Baldelli P, Taibi A, Tuffanelli A, Gilardoni M C and Gambaccini M 2005 A prototype of a quasi-monochromatic system for mammography applications *Phys. Med. Biol.* **50** 2225–40

Bernhardt P, Mertelmeier T and Hoheisel M 2006 X-ray spectrum optimization of full-field digital mammography: simulation and phantom study *Med. Phys.* **33** 4337–49

Bliznakova K, Sechopoulos I, Buliev I and Pallikarakis N 2012 BreastSimulator: a software platform for breast x-ray imaging research *J. Biomed. Graph. Comput.* **2** 1–14

Bliznakova K, Speller R, Horrocks J, Liaparinos P, Kolitsi Z and Pallikarakis N 2010 Experimental validation of a radiographic simulation code using breast phantom for x-ray imaging *Comput. Biol. Med.* **40** 208–14

Boone J M 1998 Spectral modeling and compilation of quantum fluence in radiography and mammography *Proc. SPIE, Medical Imaging 1998: Physics of Medical Imaging* (*San Diego, July 24*) vol 3336 pp 592–601

Boone J M 2002 Normalized glandular dose (DgN) coefficients for arbitrary x-ray spectra in mammography: computer-fit values of Monte Carlo derived data *Med. Phys.* **29** 869–75

Boone J M, Fewell T R and Jennings R J 1997 Molybdenum, rhodium, and tungsten anode spectral models using interpolating polynomials with application to mammography *Med. Phys.* **24** 1863–74

Dance D R 1990 Monte carlo calculation of conversion factors for the estimation of mean glandular breast dose *Phys. Med. Biol.* **35** 1211–19

Dance D R, Skinner C L, Young K C, Beckett J R and Kotre C J 2000a Additional factors for the estimation of mean glandular breast dose using the UK mammography dosimetry protocol *Phys. Med. Biol.* **45** 3225–40

Dance D R, Thilander A K, Sandborg M, Skinner C L, Castellano I A and Carlsson G A 2000b Influence of anode/filter material and tube potential on contrast, signal-to-noise ratio and average absorbed dose in mammography: a Monte Carlo study *Br. J. Radiol.* **73** 1056–67

Diekmann F *et al* 2004 Near monochromatic x-rays for digital slot-scan mammography: initial findings *Eur. Radiol.* **14** 1641–6

Dobbins J T 2009 3rd Tomosynthesis imaging: at a translational crossroads *Med. Phys.* **36** 1956–67
Feng S S and Sechopoulos I 2012 Clinical digital breast tomosynthesis system: dosimetric characterization *Radiology* **263** 35–42
Hammerstein G R, Miller D W, White D R, Masterson M E, Woodard H Q and Laughlin J S 1979 Absorbed radiation dose in mammography *Radiology* **130** 485–91
Hintsala H, Bliznakova K, Pallikarakis N and Jämsä T 2010 Modelling of irregular breast lesions *World Congress on Medical and Physics Biomedical Engineering IFMBE Proc.* (*Munich, Germany, 7–12 Sep. 2009*) vol 25 ed O Dössel and W Schlegel (Berlin: Springer) pp 2024–7
Hoheisel M, Lawaczeck R, Pietsch H and Arkadiev V 2005 Advantages of monochromatic x-rays for imaging *Proc. SPIE* vol 5745 pp 1087–95
Lazos D, Bliznakova K, Kolitsi Z and Pallikarakis N 2003 An integrated research tool for x-ray imaging simulation *Comput. Methods Programs Biomed.* **70** 241–51
Malliori A, Bliznakova K, Speller R D, Horrocks J A, Rigon L, Tromba G and Pallikarakis N 2012 Image quality evaluation of breast tomosynthesis with synchrotron radiation *Med. Phys.* **39** 5621–34
Muller B, Schlattl H, Gruner F and Hoeschen C 2011 A laser-driven undulator x-ray source: simulation of image formation and dose deposition in mammography *Medical Imaging 2011: Physics of Medical Imaging (Lake Buena Vista, Florida, February 2011)* vol 7961 pp 796106
Niklason L T *et al* 1997 Digital tomosynthesis in breast imaging *Radiology* **205** 399–6
Poplack S P, Tosteson T D, Kogel C A and Nagy H M 2007 Digital breast tomosynthesis: initial experience in 98 women with abnormal digital screening mammography *Am. J. Roentgenol.* **189** 616–23
Thilander-Klang A C, Ackerholm P H, Berlin I C, Bjurstam N G, Mattsson S L, Mansson L G, von Scheele C and Thunberg S J 1997 Influence of anode-filter combinations on image quality and radiation dose in 965 women undergoing mammography *Radiology* **203** 348–54
Yang X, Sechopoulos I and Fei B 2011 Automatic tissue classification for high-resolution breast CT images based on bilateral filtering *Medical Imaging 2011: Image Processing (Lake Buena Vista, Florida, February 2011)* vol 7962 pp 79623H
Yang X, Wu S, Sechopoulos I and Fei B 2012 Cupping artifact correction and automated classification for high-resolution dedicated breast CT images *Med. Phys.* **39** 6397–406
Yi Y, Lai C J, Han T, Zhong Y, Shen Y, Liu X, Ge S, You Z, Wang T and Shaw C C 2011 Radiation doses in cone-beam breast computed tomography: a Monte Carlo simulation study *Med. Phys.* **38** 589–97
Yoon K H, Kwon Y M, Choi B J, Son H H, Ryu C W, Chon K S, Park S H and Juhng S K 2012 Monochromatic x-rays for low-dose digital mammography: preliminary results *Invest. Radiol.* **47** 683–7
Zyganitidis C, Bliznakova K and Pallikarakis N 2007 A novel simulation algorithm for soft tissue compression *Med. Biol. Eng. Comput.* **45** 661–9